Protoplasma (2015) 252:1475–1486
DOI 10.1007/s00709-015-0777-6

ORIGINAL ARTICLE

Confocal laser scanning microscopy elucidation of the micromorphology of the leaf cuticle and analysis of its chemical composition

Pavani P. Nadiminti · James E. Rookes · Ben J. Boyd · David M. Cahill

Received: 2 December 2014 / Accepted: 9 February 2015 / Published online: 25 February 2015

Abstract Electron microscopy techniques such as transmission electron microscopy (TEM) and scanning electron microscopy (SEM) have been invaluable tools for the study of the micromorphology of plant cuticles. However, for electron microscopy, the preparation techniques required may invariably introduce artefacts in cuticle preservation. Further, there are a limited number of methods available for quantifying the image data obtained through electron microscopy. Therefore, in this study, optical microscopy techniques were coupled with staining procedures and, along with SEM were used to qualitatively and quantitatively assess the ultrastructure of plant leaf cuticles. Leaf cryosections of *Triticum aestivum* (wheat), *Zea mays* (maize), and *Lupinus angustifolius* (lupin) were stained with either fat-soluble azo stain Sudan IV or fluorescent, diarylmethane Auramine O and were observed under confocal laser scanning microscope (CLSM). For all the plant species tested, the cuticle on the leaf surfaces could be clearly resolved in many cases into cuticular proper (CP), external cuticular layer (ECL), and internal cuticular layer (ICL). Novel image data analysis procedures for quantifying the epicuticular wax micromorphology were developed, and epicuticular waxes of *L. angustifolius* were described here for the first time. Together, application of a multifaceted approach involving the use of a range of techniques to study the plant cuticle has led to a better understanding of cuticular structure and provides new insights into leaf surface architecture.

Keywords Confocal laser scanning microscopy (CLSM) · Optical microscopy · Cuticle · Epicuticular waxes · Micromorphology · Image analysis

Handling Editor: Adrienne R. Hardham

Electronic supplementary material The online version of this article (doi:10.1007/s00709-015-0777-6) contains supplementary material, which is available to authorized users.

P. P. Nadiminti · J. E. Rookes · D. M. Cahill (✉)
School of life and Environmental Sciences, Centre for Chemistry and Biotechnology, Deakin University, Geelong Campus at Waurn Ponds, Geelong, VIC 3217, Australia
e-mail: david.cahill@deakin.edu.au

B. J. Boyd
Drug Delivery, Disposition and Dynamics Monash Institute of Pharmaceutical Sciences, Monash University Parkville Campus, 381 Royal Parade, Parkville, VIC 3052, Australia

Introduction

The extracellular surface of plant leaves is covered by a complex hydrophobic layer, the cuticle, which reduces leaf water loss and ultraviolet light incidence and which has roles in protection against extreme temperatures, pathogens, and herbivores (Riederer 2007; Serrano et al. 2014; Yeats and Rose 2013). To understand the role of the cuticle, its nanomorphology and micromorphology have been investigated using a range of techniques including transmission electron microscopy (TEM) (Guzmán et al. 2014b), scanning electron microscopy (SEM) (Xue et al. 2014), and fluorescence and bright field microscopy (Buda et al. 2009). Similarly, the chemical composition of the cuticle has been examined via gas chromatography (Jetter et al. 2007) and to a lesser extent through the use of spectroscopy (Chen et al. 2005) and nuclear magnetic resonance (Chen and Schnoor 2009). The use of gas chromatography has enabled the isolation and detection of a diverse array of hydrophobic long chain carbon compounds including those containing multiple functional groups,

terpenoids, phenolics, triglycerides, and tochopherols that make up the cuticle (Jetter et al. 2007; Ménard et al. 2014). We have applied confocal laser scanning microscopy (CLSM) in conjunction with wide-field fluorescence microscopy and SEM to further elucidate the micromorphology of the cuticle of three crop species.

TEM has been instrumental in showing in a wide range of plants, the variation in ultrastructure at very high resolution of the cuticle of plant organs including leaves, stems and flowers and in certain cuticular mutants (Jeffree 2007; Zhou et al. 2014). Though TEM imaging is capable of achieving high resolution of cuticular ultrastructure, it is not without limitations. TEM imaging requires extensive sample preparation (Wilson and Bacic 2012) during which the cuticle may be modified from its native state. For example, it was recently reported that the methods used for sample preparation for subsequent TEM imaging can have a substantial effect on the ultrastructure of the cuticle and its interpretation on the leaves of *Eucalyptus globulus*, *Pyrus communis* (pear), and *Populus* sp. (poplar) (Guzmán et al. 2014a). In contrast to TEM, SEM has been principally used to study the distribution of epicuticular waxes (Go et al. 2014; Nadiminti et al. 2013). For example, SEM has been used to investigate damage to wax micromorphology following the spray application of agrochemical surfactants on weeds (Falk et al. 1994) and crop plants (Gonthier et al. 2010; Tamura et al. 2001).

The use of the fat-soluble azo stain, Sudan IV (Calbiani et al. 2004) and the fluorescent, diarylmethane Auramine O (Poulios et al. 2000) in conjunction with bright field and wide-field fluorescence/CLSM offers a new approach for the visualization of plant cuticles. Previously, Sudan IV had only been used to examine cuticle micromorphology on the leaves of *Fragaria* sp. (Lisek et al. 2002) and *Cycas* sp. (Griffith et al. 2014), while Auramine O was used for the examination of the cuticle of anthers of *Arabidopsis thaliana* (Chaudhury et al. 1994; Peirson et al. 1996) and leaves of *Zea mays* (Lequeu et al. 2003) and *Triticum turgidum* (Rascio et al. 2014). Similarly, leaf cuticle micromorphology of *Photinia serrulata* was examined using Auramine O and two-photon confocal scanning laser microscopy (Li and Chen 2014). These stains have also been used to characterize the cuticle on the fruit pericarp of *Solanum lycopersicum* in several studies (Buda et al. 2009; Czerednik et al. 2012; Domínguez et al. 2008). None of these studies, however, provide a detailed investigation of the arrangement of leaf cuticular layers. It is therefore clear that the potential of these stains coupled with the use of optical microscopy to examine the cuticle is yet to be fully realized.

The chemical makeup of the cuticle is complex with the presence of long chain aliphatic carbon compounds including fatty acids, C16 and C18 ω-hydroxy fatty acids, primary and secondary alcohols, aldehydes, ketones, alkanes, and esters (Chen et al. 2008; Kunst and Samuels 2003). Terpenoids, phenolics, and polysaccharides have also been found to be associated with plant cuticles (Yeats and Rose 2013; Jetter et al. 2007). The distribution of chemical compounds often vary developmentally (Jetter and Schaffer 2001) and between the cuticle surfaces of different organs such as fruits, stems, and adaxial/abaxial leaf planes of the same plant (Buschhaus et al. 2007; Jenks et al. 1995). The change in the chemical profile thus leads to a corresponding effect on the epicuticular wax micromorphology (Jenks et al. 1995).

In this paper, we examine the micromorphology of the cuticle and its chemical composition and detail the epicuticular wax micromorphology for three crop plants, *Triticum aestivum* (Wheat), *Z. mays* (Maize), and *Lupinus angustifolius* (Lupin). We have found that by using CLSM in conjunction with the lipophilic stains, Sudan IV and Auramine O, that it is possible to differentiate individual cuticular layers to high resolution. The cuticle on leaves of the plants selected for study was resolved into the cuticle proper (CP), external cuticular layer (ECL), and the internal cuticular layer (ICL). The micromorphology of epicuticular waxes was also investigated using SEM imaging, and a novel image analysis procedure was developed to provide a technique for quantification of epicuticular wax micromorphology. Finally, we analyzed the long-chain soluble aliphatic wax components of the cuticle of each species to examine the relationship between composition and structure of the epicuticular waxes.

Materials and methods

Plant growth and maintenance

T. aestivum cultivar Wyalkatchem (a gift from Nufarm Australia Limited, Laverton North, VIC, Australia), *Z. mays* variety Early Leaming (Eden seeds, Lower Beechmont, QLD, Australia), and *L. angustifolius* variety Wonga (Naracoorte seeds, Naracoorte, SA, Australia) seeds were sterilized by continuous stirring in 80 % (*v*/*v*) ethanol for 30 s. The seeds were then directly transferred to 2 % (*v*/*v*) sodium hypochlorite solution in which they were again stirred for 2 min. Seeds were immediately washed in sterile distilled water (sdH_2O) five times. Seeds were subsequently germinated on cotton wool saturated with water in a plastic tray and placed in a growth cabinet (Thermoline Scientific, Wetherill Park, NSW, Australia) maintained at a temperature of 21 °C under high pressure sodium lights (approximately 300 μmol/m^2/s) with 16/8 light/dark photoperiod for 2 days. Healthy seedlings were then transferred to sterile potting mix (Potmate Premium Potting Mix, Debco, Tyabb, VIC, Australia) in 10 cm in diameter × 10-cm-high plastic pots that were regularly watered and maintained under the same conditions described for germination.

Arabidopsis thaliana is known for the absence of epicuticular wax crystals on the leaf surface (Jenks et al. 1995; Nadiminti et al. 2013). *A. thaliana* was therefore used as a control for the experimental procedures followed for SEM and image analysis and was also included in gas chromatography analysis. *A. thaliana* ecotype Col-0 seeds obtained from Lehle seeds (Round Rock, Texas, USA) were carefully transferred to 1.5-ml microfuge tubes for surface sterilization. Seeds were sterilized in 50 % (*v*/*v*) ethanol and 1.5 % (*w*/*v*) hydrogen peroxide (Sigma-Aldrich, Sydney, NSW, Australia) for 5 min with regular shaking. After centrifugation for 20 s, the supernatant was discarded, and the seeds were rinsed in sdH_2O at least three times. A solution of 0.15 % (*w*/*v*) bacteriological agar was added to the seeds before transferring them to 90-mm Petri plates containing MS basal media (Sigma-Aldrich, Sydney, NSW, Australia) 3 % (*w*/*v*) sucrose along with 0.8 % (*w*/*v*) bacteriological agar (Sigma-Aldrich) adjusted to pH 5.7. Following stratification for 48 h at 4 °C, seeds were maintained in a growth cabinet (Thermoline Scientific) for 14 days at 21 °C, under cool white fluorescent light at an intensity of 100 μmol/m^2/s, with a 16/8 photoperiod. Healthy seedlings were then carefully transferred to 4 cm in diameter × 8-cm-high plastic pots containing sterile potting mix (Potmate Premium Potting Mix, Debco).

Sample fixation and cryo-sectioning

After 21 days of growth (7 days for *A. thaliana*), healthy leaves from plants were excised and washed in dH_2O. The leaves were then fixed following the method described by Buda et al. (2009) with several modifications. Briefly, leaf tissue was floated on FAA fixative containing 37 % formaldehyde (*v*/*v*), 5 % glacial acetic acid (*v*/*v*), 45 % ethanol (*v*/*v*), 45 % distilled water (*v*/*v*), and vacuum-infiltrated for 15 min. Leaf tissue was transferred to 4 °C and left overnight in fresh FAA fixative. For cryoprotection, the tissue was vacuum-infiltrated for 15 min in 10 % sucrose (*w*/*v*) in 100-mM phosphate-buffered saline (PBS) containing 11.5 g/l Na_2HPO_4, 2 g/l NaH_2PO_4, 90 g/l NaCl, at pH 7.2, followed by a 15-min vacuum infiltration in 20 % sucrose (*w*/*v*) in 100 mM PBS. The tissue was subsequently rinsed in embedding medium (Tissue-tek OCT compound, ProSciTech Pty Ltd., Thuringowa, QLD, Australia) and placed in cryomolds (15 mm × 15 mm × 5 mm, ProSciTech) containing fresh embedding medium. The cryomolds were then very slowly immersed in liquid nitrogen, and the frozen cryomolds were stored at −80 °C until further processing. A Cryostat (Microm HM550 OMP, Thermo Scientific, Scoresby, VIC, Australia) was employed to cut transverse sections of 5–30-μm thickness. The sections were carefully transferred to gelatine-coated slides and stored at 4 °C until further use.

Staining of tissue sections

Three stains, namely, Sudan IV, Auramine O, and Calcofluor white M2R (Sigma-Aldrich), were used to facilitate visualization of the cuticle and cell wall in bright field and fluorescence microscopy. Sudan IV stain was prepared by dissolving 0.1 % Sudan IV (*w*/*v*) in isopropyl alcohol. This solution was diluted with dH_2O water in a ratio of 3:2 before filtering it through a 0.4-μm syringe filter (GE Healthcare Pty. Ltd. Australia, Rydalmere, NSW, Australia). Cryosections were then stained for 10 min before gently washing away unbound stain with 50 % isopropyl alcohol. The sections were then gently washed with dH_2O mounted on a microscope slide with a cover slip, and the edges were sealed with commercially available transparent nail polish (Buda et al. 2009).

Auramine O stain was prepared by dissolving 0.1 % Auramine O (*w*/*v*) in 50 mM Tris/HCl at pH 7.2. The sections were stained in freshly prepared stain for 15 min. After washing the sections with dH_2O, they were mounted in DABCO (Sigma-Aldrich) or 50 % glycerol (*v*/*v*) on a microscope slide, and a coverslip was sealed to the slide with transparent nail polish (Buda et al. 2009). Calcofluor white M2R stain was prepared by dissolving 0.1 % (*w*/*v*) in dH_2O. After staining with Calcofluor for 2 min and gently rinsing with dH_2O, the cryosections were transferred to microscope slides and then stained with Auramine O. Mounting of the slides was performed as described above for Auramine O.

Bright field and fluorescence microscopy

Bright field microscopy and epifluorescence microscopy were performed using an Axioskop 2 mot plus microscope (Zeiss, Göttingen, Germany). A digital camera attached to the microscope was employed to capture images. For collecting ultraviolet light-induced epifluorescence, a filter with 365-nm excitation and 420-nm emission bands was used, and for blue light, a filter with 450–490-nm excitation and 520-nm emission bands was used. Confocal microscopy was performed using a Leica TCS-SP5 microscope (Leica Microsystems Pty Ltd., North Ryde, NSW, Australia) with image capture software (LAS AF software version: 2.6.3.8137). Auramine O was excited at 458 nm using an argon laser, and emission was collected between 491 and 563 nm. Calcoflour was excited using a laser from a near-UV diode at 405 nm, and emission was collected between 415 and 448 nm (Buda et al. 2009). Prior to z-stacking at a magnification of 1000×, 2D imaging was performed, and the z-stacks with a step size of 0.5 μm were collected. Image analysis software (Adobe® Photoshop® CS6 version 13.0 × 64, Adobe Systems Pty. Ltd., Sydney, NSW, Australia) was used to prepare the images.

Sample preparation and gold coating for SEM

Fresh leaves were collected from plants that were grown as described earlier. A healthy, mature leaf was randomly sampled from each plant giving a total of four leaves per species. The excised leaves were maintained at room temperature for 24 to 48 h to slowly reduce the water content (Pathan et al. 2008). A small area of 3×3 mm^2 was cut from each leaf using a clean scalpel blade. The tissue was mounted with the adaxial side exposed for analysis on a clean aluminum stub using an adhesive conducting carbon tape and stored within a vacuum chamber until further use. The samples were coated with gold palladium for 60–120 s at 40 mA (BAL-TEC Sputter Coater SCD 050, Scotia, NY, USA) before performing scanning electron microscopy (Supra 55 VP, Carl Zeiss Pty Ltd., NSW, Australia). A voltage between 5 and 10 kV was maintained while imaging the samples. For each plant species, a minimum of 35 images was obtained.

Image analysis

A freely available software package ImageJ (version 1.46r) (Schneider et al. 2012) was used to calculate the percentage area of crystalline epicuticular wax cover and total perimeter of wax crystals on SEM images. For calculating percentage area of wax crystal cover, ten images, 1024×768 pixels in size, were randomly selected for each species and converted to 8-bit images to adjust the threshold in imageJ software. The images were then processed in imageJ to reduce the noise using the "despeckle" function. The percentage area and perimeter of the epicuticular wax crystals were then calculated using the "analyse particles" function in the software for each image. Data obtained was statistically analyzed using a commercial software package (IBM SPSS Statistics 21, IBM Australia Ltd, St Leonards NSW, Australia).

Gas chromatography

To extract the cuticular waxes from the surface of leaves, 200 mg of fresh mature leaf tissue from each species was dipped separately in 2-ml chloroform containing 100 μg of triacontane (Sigma-Aldrich) for 15 s at room temperature (Broun et al. 2004). After removing the plant tissue, chloroform was removed under a continuous stream of nitrogen gas. Prior to derivatization, the extract was dissolved in 100 μl of *N*,*O*-bis (trimethylsilyl) trifluroacetamide with 1 % trimethylchlorosilane (Sigma-Aldrich) and 100 μl pyridine (Sigma-Aldrich). Derivatization was carried out at 100 °C for 1 h. To analyze the samples, an HP5MS (30 m, 0.25 mm i.d, 0.25-μm film thickness; Supelco) column fitted to an Agilent 6890 gas chromatograph running on a flame ionization detector was used. The initial temperature of the oven was set at 150 °C followed by ramping at 4 °C/min to 320 °C (10 min hold). At an injection temperature of 280 °C, a sample volume of 1 μl was injected, and flow rate of helium gas was adjusted at 1.5 l/min (Hannoufa et al. 1993; Millar et al. 1999). Peaks were identified by comparing the retention times with known commercial standards (Sigma-Aldrich). Commercially obtained standards for even numbered long chain saturated fatty acids between C16 to C30, even numbered long chain primary alcohols between C24 to C30, and long chain alkanes between C20 to C40 were used to identify respective peaks (Hannoufa et al. 1993; Millar et al. 1999).

Results

Micromorphology of the cuticle on the leaves of *T. aestivum*, *Z. mays*, and *L. angustifolius*

While Sudan IV and Auramine O were used to stain the cuticle on the leaf cryosections of *T. aestivum*, *Z. mays*, and *L. angustifolius*, Calcoflour was used to selectively stain cell walls, in which polysaccharides are the major constituents (Herth and Schnepf 1980). Following Sudan IV staining, the cuticle was observed as a continuous bright red to pink layer on both adaxial and abaxial surfaces of the leaves of *T. aestivum* (Fig. 1a, b), and cuticular overhangs were consistently observed over the stomatal guard cells. To resolve the cuticle into different layers, wide-field fluorescence and CLSM were performed on *T. aestivum* leaf transverse sections after staining with Auramine O. Under wide-field fluorescence microscopy, only the cuticle proper (CP) was distinctly observed external to the cell wall (CW) on leaf edges and epidermal cell layers (Fig. 1c, d). Auramine O staining and observations under CLSM resolved distinct layers of the cuticle, CP, external cuticular layer (ECL), and internal cuticular layer (ICL). The CP was present as a conspicuous bright layer over a dull fluorescent ECL (Fig. 1e, f). ECL was sandwiched between two bright layers, CP and ICL, and ICL was further observed to be continuous with the underlying cell wall of the epidermis, and its boundaries could not be delineated (Fig. 1f). Anticlinal pegs were highly cuticularized giving rise to an increase in the thickness of the cuticle in the anticlinal cell junctions in comparison to the cuticle on periclinal cell regions of the epidermis (Fig. 1f). Cuticular overhangs observed earlier with Sudan IV staining were present as brightly fluorescent projections over the guard cells of stomata. Double staining *T. aestivum* cryosections with Auramine O and Calcofluor followed by fluorescence microscopy (Fig. 1g, h) could only resolve the cuticle from the cell wall region. CLSM, however, enabled the identification of the cell wall region in relation to the stacked layers of cuticle CP, ECL, and ICL (Fig. 1i, j). The cuticle micromorphology on the leaf cross sections of *L. angustifolius* (Fig. 2) and *Z. mays* (Fig S1) was consistent with that of *T. aestivum*, while the anticlinal pegs of

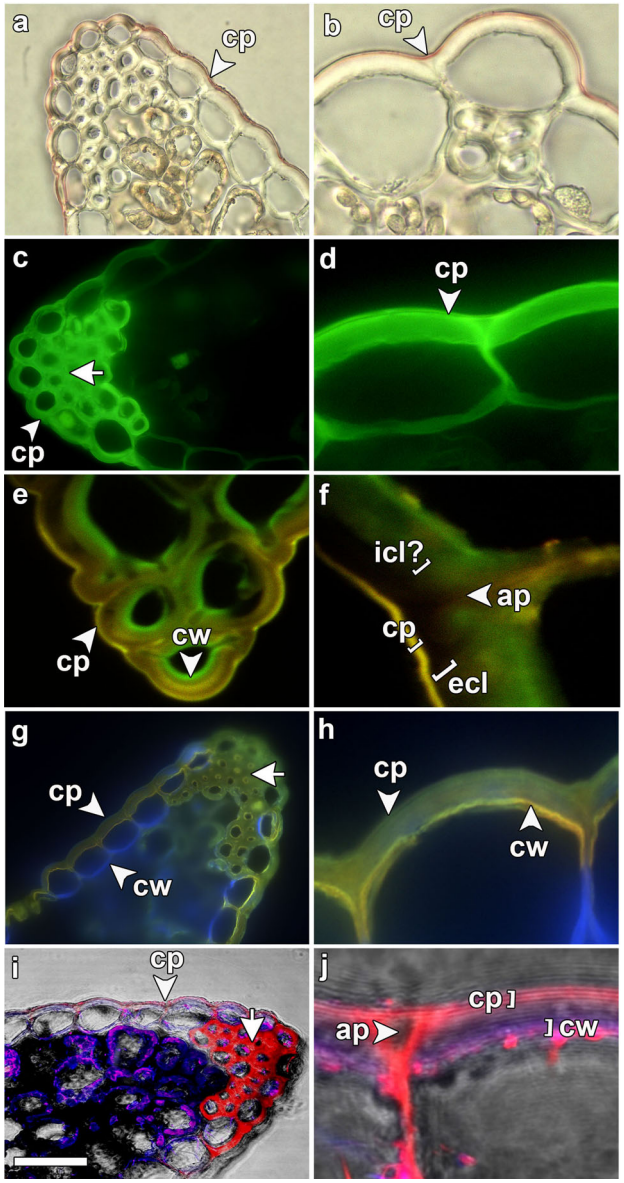

Fig. 1 Transverse sections of leaves of *T. aestivum* observed using light microscopy (**a**,**b**), wide-field fluorescence microscopy (**c**, **d**, **g**, **h**), and CLSM (**e**, **f**, **i**, **j**) following staining with Sudan IV, Auramine O, or Calcofluor M2R. **a** Leaf edge and **b** central lamina, stained with Sudan IV. Cuticle proper (cp) was seen as a bright pink to red layer on the epidermal cells external to the cell wall. **c**, **d** Following staining with Auramine O only cp could be seen as a bright layer on the cell periphery. At leaf edge (**c**), the cells below the epidermis appear to be cuticularized (shown by an *arrow*). In **d**, cp is shown on epidermal cells. **e**, **f** Overlay of Auramine O channel and autofluorescence channel of stained samples clearly resolved the layers of the cuticle. **f** The dull external cuticular layer (ecl) was sandwiched between brightly fluorescent cp and internal cuticular layer (icl). The boundaries of icl could not, however, be delineated. **g**, **h** Dichromatic staining using both Auramine O and Calcofluor was performed to resolve the cell wall (cw) from cuticular layers. The cuticular region is a bright yellow color while cw regions are seen either yellow/green or blue in color. **g** The cw region adjacent to parenchymal layers is blue in color, while **h** the cw region that is continuous with the cuticle is yellow in color. **i, j** Under CLSM, the cell wall regions could be clearly resolved from the cuticule. **i** Leaf edge, **j** epidermal cells of leaf lamina. *Scale bar* **a**, **g**, **i**= 30 μm; **c**=20 μm; **e**=7.5 μm; **b**, **d**, **h**, **j**=5 μm; **f**=2.5 μm

L. angustifolius epidermal cells did not extend into the anticlinal cell junctions (Fig. 2b).

For CLSM, 3D reconstruction provided new insights into the spatial distribution of cuticular layers and cellulosic material on the epidermal cells. The cuticle on the leaves of *T. aestivum*, *Z. mays*, and *L. angustifolious* was resolved into stratified layers of CP, ECL, and ICL (Fig. 3) although the identification of ICL was not always well resolved. The 2D (Fig. 3) and 3D (Fig S2) images of *T. aestivum* and *Z. mays* showed a similar pattern for the deposition of cuticular material deep in the anticlinal cell junctions (Fig. 3; Fig S2 a, b, d, e, g, and h) when compared with *L. angustifolious* (Fig. 3; Fig S2 c, f, and i). There was a significant decrease in the fluorescence intensity for the optical sections collected at the deeper optical plains of the cryosection (Fig S2).

Micromorphology of epicuticular waxes on the leaves of *T. aestivum*, *Z. mays*, and *L. angustifolius*

SEM studies carried out on the leaves of *T. aestivum* and *L. angustifolius* displayed a single type of epicuticular wax crystal on their surface. By contrast, *Z. mays* exhibited three different types of epicuticular wax crystals on its phylloplane. A classification of epicuticular waxes based on the epicuticular wax classification system proposed by Barthlott et al. (1998) was conducted. Using this classification system, the wax crystals on leaves of *T. aestivum*, *Z. mays*, and *L. angustifolius* were identified as crystalloids and were all within the category "plates and platelets." The crystalloids were further identified into three subgroups, namely, "entire platelets, irregular platelets, membranous platelets and plates." Entire platelets (EP) have a continuous margin, have an irregular shape, and are larger in size than other crystalloids (Fig. 4a, b; Fig. 5). Irregular crenate platelets (ICP) were entire platelets but with crenation of the margins and were quite similar to the EP (Fig. 4c, d; Fig. 5). Membranous platelets (MP) were entire platelets or crenate platelets with a membranous extension (Fig. 4 e, f; Fig. 5).

There was a dense network of the epicuticular waxes on leaves of *T. aestivum* identified as ICP (Fig. 5a), which were interspersed with regions that were devoid of wax platelets (Fig S3 a). Epicuticular waxes appeared to be fused with adjacent wax platelets forming complex continuous structures that were consistently irregular in arrangement (Fig. 5a). Most of the fused platelets were perpendicular to the surface of the leaf, while others were positioned at an angle to the vertical (Fig. 5a; Fig S3c). Individual wax crystals could only be resolved under higher magnification (Fig. 5a; Fig S3 a–c). Though the shape of wax platelet was consistent with epicuticular wax classification, the size was, by contrast, very different from that previously reported. The reported size for irregular platelets in the literature was 1–10 μm in height (Barthlott et al. 1998), but in the current study, the average

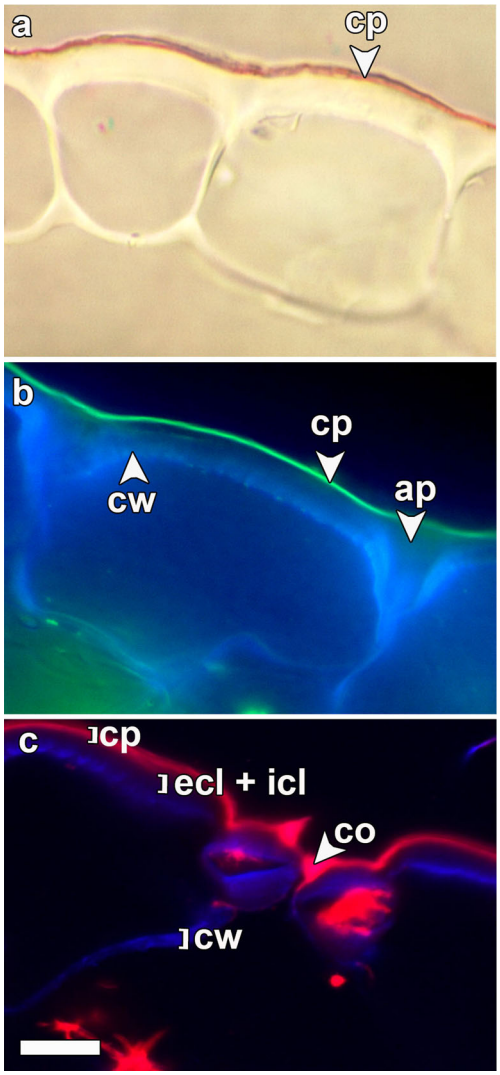

Fig. 2 Ultrastructure of the cuticle on *L. angustifolius* leaf surface. Similar to the Sudan IV staining on the *T. aestivum*, **a** the cuticle proper (cp) on the leaf epidermis is a bright continous pink to red layer under bright-field microscopy. **b** Wide-field fluorescence and **c** CLSM microscopy of dichromatically stained leaf transverse sections resolve the layers of the cuticle. cp is the bright pink layer external to the epidermal cells. Unlike *T. aestivum* and *Z. mays*, the anticlinal pegs (ap) did not extend into the cell junctions. Using CLSM, the cell wall (cw) and cp is clearly distinguished from cuticular layers ecl and icl. The cuticular overhangs (co) on the stomatal guard cells can be clearly seen. *Scale bar* **a**= 15 μm; **b**=10 μm; **c**=7.5 μm

size measured was less than 170 nm (or 0.17 μm) in height, while the thickness of the platelet was approximately 25 nm.

Z. mays also had a dense covering of epicuticular wax crystals on its phylloplane, and the presence of EP, MP, and ICP was confirmed using SEM (Fig. 5b; Fig S3 d–f). Due to the presence of different types of wax crystals arranged in a random array on the same plane, the arrangement of the crystalloids was complex when compared to that of *T. aestivum*. Most of the crystalloids were arranged perpendicular to the underlying wax layer while some were arranged at an angle. The occurrence of different forms of crystalloids on a single phylloplane was earlier described as syntopism (Barthlott et al. 1998) (Fig. 5b). The size of crystalloids was much varied ranging from a few to several hundred nanometers (for entire platelets). The thickness was approximately 25 nm and similar to that of *T. aestivum* wax crystals.

The arrangement of the epicuticular wax crystals on *L. angustifolius* was very similar to that of *T. aestivum* and *Z .mays*, with a dense cover of crystalloids (Fig. 5c; Fig S3 g–i). Only MP could be identified on the phylloplane of *L. angustifolius*. The height and thickness of the platelets were approximately 225 nm and 41 nm, respectively. The arrangement of the MP was dense within the region around the stomatal wax chimney clear of any wax crystalloids and was unique for *L. angustifolius* (Fig S3g, h, and i).

A. thaliana was previously shown not to contain epicuticular wax crystals on the leaf surface and was instead shown to be covered with an epicuticular wax sheath or amorphous wax sheath (Jeffree 2007; Jenks et al. 1996) (Fig. 5d; Fig S3j, k, and l).

Relative surface coverage of epicuticular wax crystals

The relative surface coverage of cuticular wax crystals was determined by a customized image analysis procedure developed through utilization of the image processing program imageJ. *T. aestivum* (24.10 %±1.30) and *L. angustifolius* (23.50 %±0.80) had a statistically similar surface coverage of cuticular wax crystals (Table 1). The percentage coverage on *Z. mays* (28.81±1.50) was higher and statistically different when compared to that of *T. aestivum*, *L. angustifolius*, and *A. thaliana*. The perimeter of epicuticular wax crystals was also calculated on the analyzed images. Except for *A. thaliana*, the perimeter on the species tested was similar to each other and was not statistically different between groups (Table 1).

The chemical composition of plant cuticular waxes

Gas chromatography was performed to analyze the compositional differences in the aliphatic compounds that form the epicuticular waxes of the different plants under study. In the wax extracts of *T. aestivum*, we could detect long chain even numbered, saturated fatty acids, and alcohols ranging, respectively, between C16 to C30 and C24 to C30 and long chain odd numbered alkanes ranging between C23 to C37 except for hentriacontane (C31 alkane) (Table 2). Of further interest, flame ionization detector (FID) intensity corresponding to octacosanol (C28 alcohol) was observed to be considerably higher than that of other peaks and is consistent with an earlier report (Koch et al. 2006). Except for

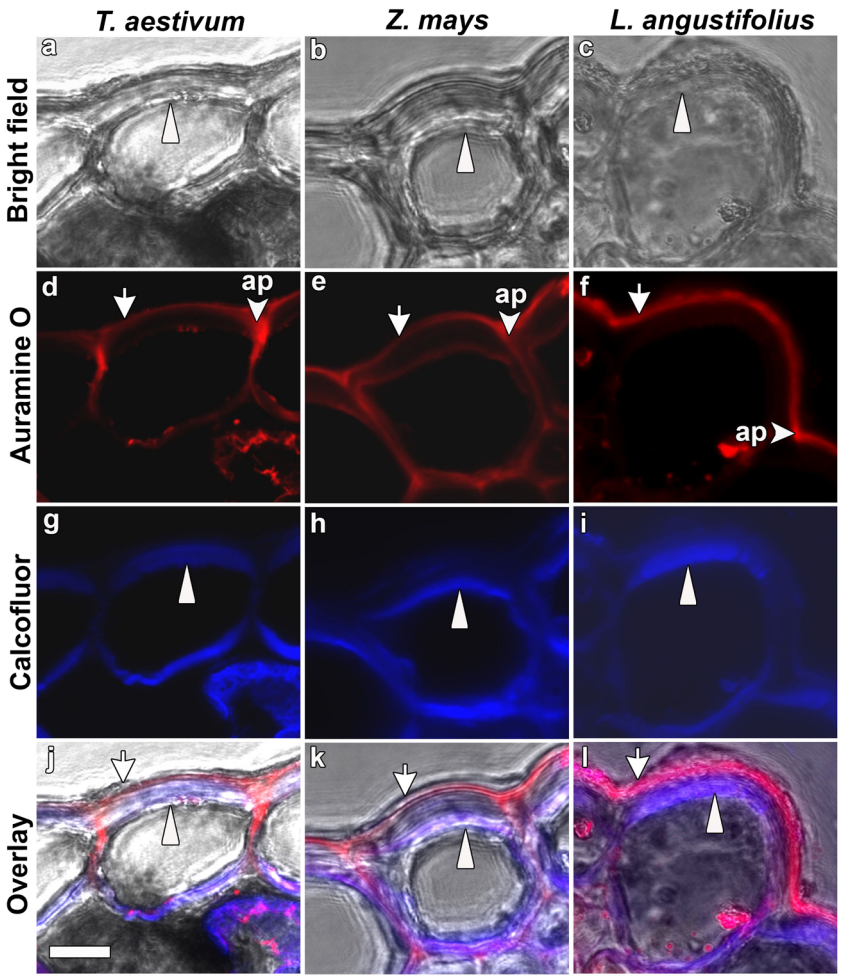

Fig. 3 Overview of the micromorphology of *T. aestivum*, *Z. mays*, and *L. angustifolius* cuticles observed under CLSM after dichromatic staining. Auramine O was used to stain the cuticle while Calcofluor stained the cellulosic regions of the leaf transverse sections. The cell wall is indicated by the *arrow heads* and cuticle with *arrows*. The brightfield (**a**, **b**, **c**) and Auramine O (**d**, **e**, **f**) channels of CLSM. **d**, **e** Cuticle stained with Auramine O was observed to be similar for *T. aestivum* and *Z. mays*. The anticlinal pegs (ap) of *T. aestivum* and *Z. mays* extend into cell junctions and appear to be cuticularized, **f** ap of *L. angustifolius* did not. **g**, **h**, **i** Calcofluor channel showing the cell wall. Overlay channel (**j**, **k**, **l**) precisely locates the position of the cuticle and the cw regions of the leaf transverse sections. *Scale bar*=5 μm

eicosanoic acid (C20 fatty acid), long chain even numbered saturated fatty acids ranging between C16 to C30 were detected along with the long chain even numbered alcohols ranging between C24 to C30 in the epicuticular wax extracts of *Z. mays* (Table 2). Like *T. aestivum*, detection of alkanes in *Z. mays* wax extracts followed the same trend (Table 2). For *Z. mays*, the FID response was contrastingly high for triacontanoic acid (C30 fatty acid). For *L. angustifolious*, saturated long chain fatty acids with even numbered carbons, namely, C16, C18, C22, C24, C28, and C30 and even numbered long chain primary alcohols C24, C26, C28, and C30, were identified (Fig. 6) (Table 2). Alkanes in the epicuticular waxes of *L. angustifolious* followed the trend observed for *T. aestivum* and *Z. mays*. The composition of *A. thaliana* leaf waxes has been extensively described for the presence of different aliphatic compounds such as fatty acids, primary alcohols, and alkanes (Go et al. 2014; Rashotte et al. 1997). *A. thaliana* was therefore used as a control for the methodology adopted for gas chromatography, and the aliphatic compounds detected for *A. thaliana* were consistent with previous reports (Jenks et al. 1995) (Table 2).

Discussion

Microscopic imaging of plant cuticles at high resolution is an essential approach for analysis of the structural organization of the cuticle. However, to date, detailed structural analysis of the cuticle using bright-field and wide-field fluorescence microscopy techniques including CLSM has been limited to *S. lycopersicum* fruits (Buda et al. 2009) and *Photinia serrulata* leaves (Li and Chen 2014). Therefore, this study used different staining procedures in combination with optical microscopy techniques to achieve high-resolution imaging of plant cuticles. Furthermore, an image analysis procedure was developed to quantify the data collected using SEM, to allow detailed analysis of the structural integrity of the wax crystals on the phylloplanes of the plants under study. Finally, the compositional differences between the cuticular wax extracts of *T. aestivum*, *Z. mays*, *L. angustifolius*, and *A. thaliana* were also investigated. Together, these results demonstrate the power of a combinatorial approach for studying the micromorphology and chemical composition of the plant cuticle.

Sudan IV staining allowed the visualization of the cuticle on epidermal cells which was observed as a continuous layer

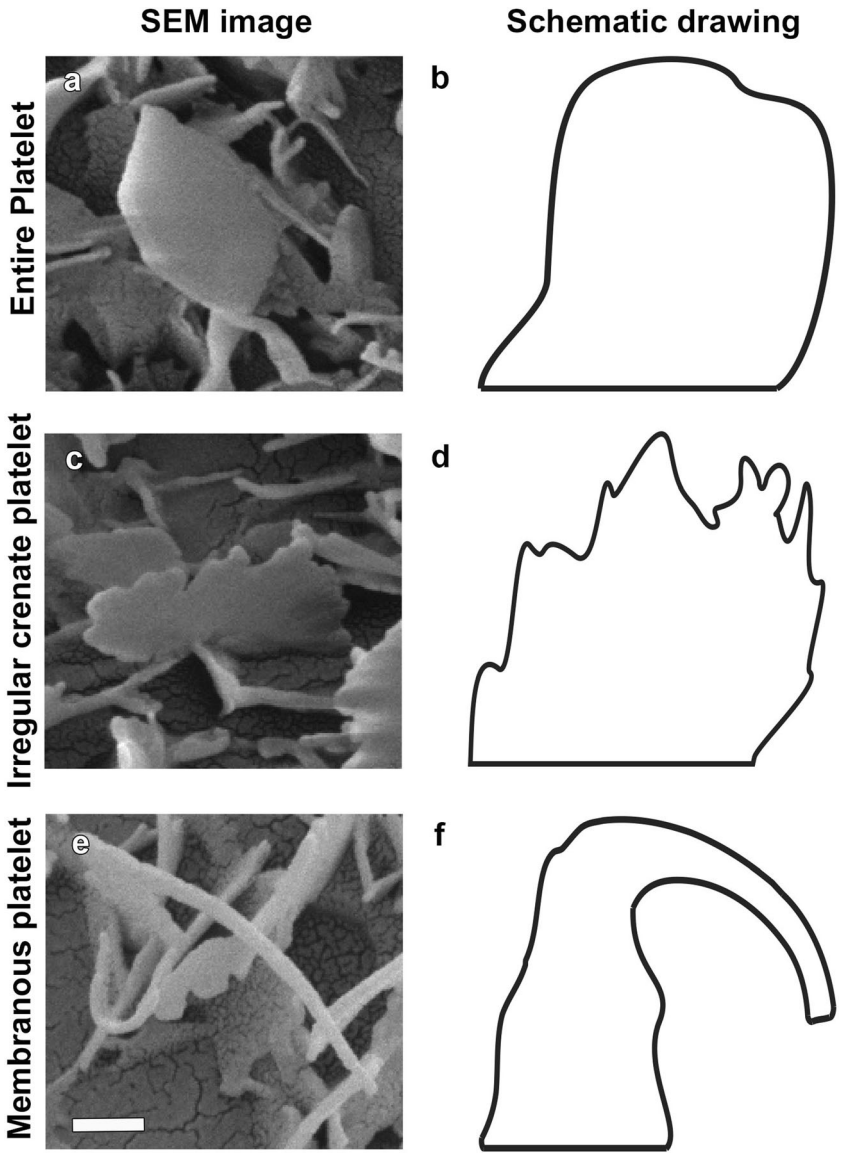

Fig. 4 SEM of typical epicuticular wax crystalloids on leaf surfaces. *The left side column* shows the scanning electron microscopy (SEM)-derived images of wax crystollids while *the right side column* shows a schematic drawing of the corresponding epicuticular wax crystolloid. **a**, **b** Entire platelet was characterized by the presence of smooth edges. **c**, **d** Irregular crenate platelets were platelets with rough edges of random shape. **e**, **f** The memberanous platelet is a crenate platelet that is sometimes irregular but often has a memberanous extension of the crystalloid. *Scale bar*=70 nm

both on adaxial and abaxial leaf surfaces. Cuticular overhangs on stomatal guard cells were consistently observed on all leaves. These overhangs form a stomatal chimney in a 3D array that covers and protects the stomatal apparatus (Barthlott et al. 1998). Confirmation of the presence of stomatal chimneys was also obtained through SEM observations further demonstrating the robustness of the adopted staining and microscopy procedures. Dichromatic staining was performed using Auramine O and Calcofluor to resolve different layers of the cuticle from the cell wall. Epidermal cells of *T. aestivum*, *Z. mays*, and *L. angustifolius* responded differently to dichromatic staining. In *T. aestivum*, yellow staining of cell wall regions adjacent to the cuticle was observed under wide-field fluorescence microscopy. This indicates that cross-talk between the two fluorophores as the cell wall was predominately blue in all other regions (Carlsson and Mossberg 1992). The cell wall region was, however, clearly resolved from the cuticular layers with CLSM. From the CLSM studies on *T. aestivum* and *Z. mays*, it was clear that the deposition of the cuticular material extended into the junctions between cells as aniticlinal pegs. For *L. angustifolius*, the cuticular material did not extend deep in the anticlinal cell junctions and was also confirmed with the 3D reconstructions. The reason for differences in cuticularization of anticlinal pegs is probably a consequence of the broad anatomical and chemical differences between eudicots and monocots used in this study.

The detailed analysis of cuticular structure presented in this study achieved through optical microscopy closely correlates with previous studies that employed TEM imaging (Jeffree 2007; Yeats et al. 2012; Guzmán et al. 2014b; Yeats and Rose 2013). While not able to provide the high magnification

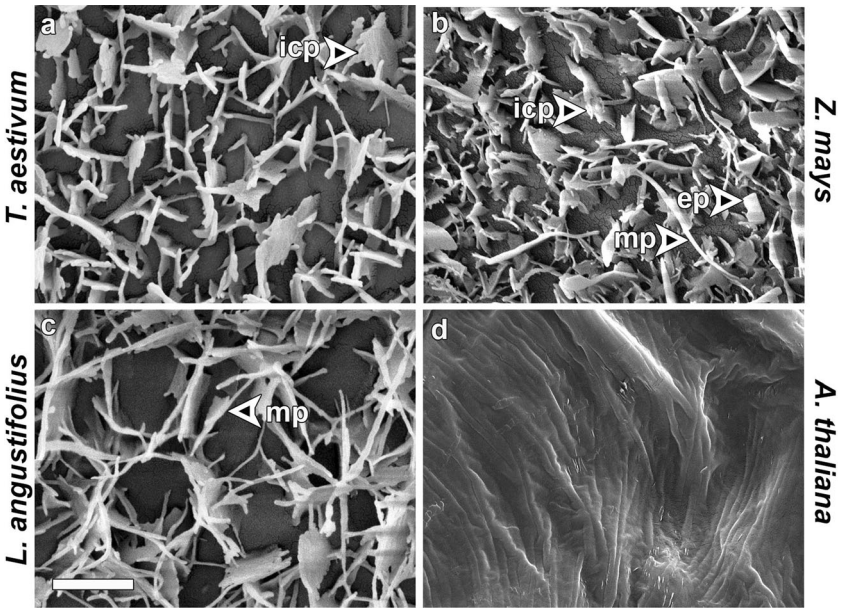

Fig. 5 SEM of epicuticular wax micromorphology on the leaves of *T. aestivum*, *Z. mays*, *L. angustifolius*, and *A. thaliana*. **a** The surface of *T. aestivum* was covered only with irregular crenate platelets (icp). **b** The phylloplane of *Z. mays* shows the presence of different types of wax crystalloids which is referred to as syntopism. Entire platelets (ep), membranous platelets (mp). **c** *L. angustifolius* leaf surface was covered solely with mp. **d** Epicuticular wax crystals were totally absent on the leaf surface of *A. thaliana* and are instead covered with an epicuticular wax sheath. *Scale bar* **a**, **b**, and **c**= 200 nm; **d**=1 μm

that TEM offers, the use of lipohillic stains Sudan IV and Auramine O enabled the detailed analysis of the leaf cuticle of various species using optical microscopy. The fixation and staining procedures described here are straightforward and less invasive than those required for TEM, although we cannot discount the possibility of minor structural artefacts from occurring. Auramine O, in particular, has a differential affinity toward the various cuticular layers such as CP, ECL, and ICL (Buda et al. 2009). Furthermore, the addition of Calcofluor provided precise localization of the cell wall of leaf epidermal cells. While the use of bright-field and wide-field fluorescence microscopy provided clear demarcation of the cuticle, the use of CLSM highlighted the cuticle in finer detail. CLSM has previously been shown to be of great benefit to subcellular level studies of plant cells, such as in visualization of the cytoskeleton (Cahill et al. 2002) and cell organelles (Hardham 2012; Ruberti et al. 2014). Our study further demonstrates the applicability of CLSM to identify structures at the micrometer and submicrometer scale in plant cells.

Table 1 Quantification of epicuticular wax micromorphology

Species	Relative surface coverage of epicuticular waxes (%)	Perimeter of wax crystals/image (nm)
T. aestivum	24.10±1.30^{b}	794.21±61.50^{a}
Z. mays	28.81±1.50^{a}	807.62±49.90^{a}
L. angustifolius	23.50±0.80^{b}	709.21±48.10^{a}
A. thaliana	2.80±0.80^{c}	1.65±0.10^{b}

The relative surface coverage of epicuticular wax crystals is shown. The percentage area of epicuticular wax crystals was calculated for each leaf from standard sized images (1024×768 pixels) of the leaf surface at the same scale

Values are mean±SD for ten images. Values followed by same letter are not statistically different, for ANOVA with Duncan's post hoc testing

Except for *A. thaliana*, the leaf surfaces of all the plants in the study were covered with a dense array of epicuticular waxes. The leaf surface of *A. thaliana* was devoid of any epicuticular wax crystals; instead, it is covered by a wax sheath (Jeffree 2007). The leaf surface of *L. angustifolius* on the other hand was covered with a dense array of MP that has, to our knowledge, not been previously described. The leading edges of these MP overlapped the adjacent platelets and contributed toward the complexity of the micromorphology. Our observations of the epicuticular wax crystalloids of *Z. mays* and *T. aestivum* were similar to those described in earlier reports (Beattie and Marcell 2002; Koch et al. 2006).

As there are few methods described to quantify the micromorphology of epicuticular waxes, a procedure was developed for the precise calculation of epicuticular wax crystalloid surface coverage utilizing a freely available software, ImageJ (Schneider et al. 2012). However, it must be appreciated that image analysis by necessity is carried out on a 2D image of 3D epicuticular waxes. The data produced is therefore representative of the wax structure but is not an actual calculation of the surface area. The percentage area value on *Z. mays* was significantly larger than that of *T. aestivum* and *L. angustifolius*, which can possibly be an outcome of the syntopic arrangement of the epicuticular waxes on the *Z. mays* phylloplane (Barthlott et al. 1998). The absence of epicuticular waxes on *A. thaliana* contributed toward the very low area value in comparison to that of *T. aestivum*, *Z. mays*, and *L. angustifolius*. From the range of percentage of values (excluding *A. thaliana*), it was evident that this method of image analysis was sensitive and able to identify the subtle

Table 2 Aliphatic long-chain carbon constituents of epicuticular waxes of four plant species

Carbon number and functional group	Systematic name	Plant species detected in
Fatty acids		
16	Hexadecanoic acid	T, Z, L A,
18	Octadecanoic acid	T, Z, L, A,
20	Eicosanoic acid	T
22	Docosanoic acid	T, Z, L
24	Tetracosanoic acid	T,Z, L, A,
26	Hexacosanoic acid	T, Z, A
28	Octacosanoic acid	T, Z, L, A,
30	Triacontanoic acid	T, Z, L, A,
Alcohol		
24	Tetracosanol	T, Z, L, A
26	Hexacosanol	T, Z, L, A
28	Octacosanol	T, Z, L, A
30	Triacontanol	T, Z, L, A
Ketones		
29	15-Nonacosanone	A
Alkanes		
23	Tricosane	T, Z, L
25	Pentacosane	T, Z, L, A,
27	Heptacosane	T, Z, L, A,
29	Nonacosane	T, Z, L, A,
31	Hentraicontane	A
33	Tritriacontane	T, Z, L
35	Pentatriacontante	T, Z, L
37	Heptatriacontane	T, Z, L

The table summarizes the aliphatic long-chain compounds identified using gas chromatography of soluble leaf wax extracts

Commercial standards were separately used to identify the corresponding peaks in the wax extracts of *T. aestivum* (T), Z. *mays* (Z), *L. angustifolius* (L), and *A. thaliana* (A)

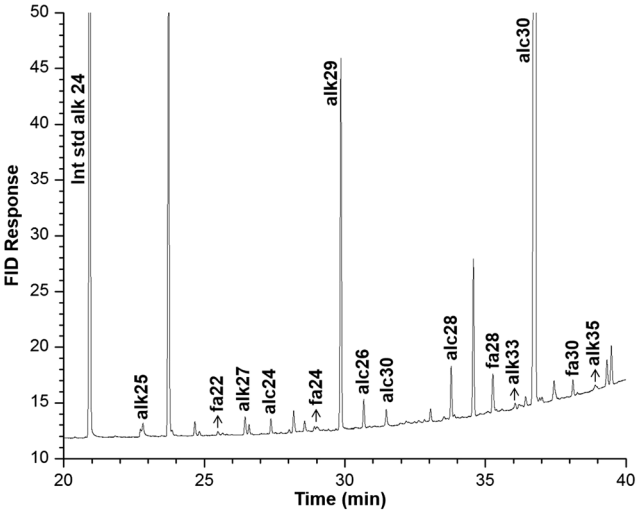

Fig. 6 Chromatogram of epicuticular waxes extracted from the leaf surface of *L. angustifolius*. Peaks are labeled with "fa" for fatty acids, "alk" for alkanes, and "alc" for alcohols. *The number prefix* represents the carbon number. For example, fa 16 indicates 16 carbon chain fatty acid. Alkane 24 was used as an internal standard (Int std)

differences between the morphological arrangement of epicuticular waxes.

The epicuticular wax plates of *T. aestivum*, *Z. mays*, and *L. angustifolius* are based on primary alcohols (Jeffree 2007; Koch et al. 2006), and we have confirmed this using gas chromatography. Octacosanol, the most abundant alcohol found in the wax extracts of *T. aestivum*, likely contributed toward the formation of ICP on leaves of this species (Koch et al. 2006). Similarly, the composition of epicuticular waxes on the surface of *Z. mays*, *L. angustifolious*, and *A. thaliana* is likely responsible for the presence of their respective type of wax micromorphology (Beattie and Marcell 2002; Jeffree 2007). For example, epicuticular waxes of members of the families Fabaceae, Myrtaceae, and Poaceae that are rich in primary alcohols are known to have a simple platelet micromorphology (Jeffree 2007). With further development of techniques to isolate epicuticular waxes alone from the phylloplanes, it may be possible to more accurately predict the fine structure of the epicuticular waxes through the analysis of the chemical composition of the cuticle.

In this study, the leaf cuticles of three plant species were visualized using various staining procedures and optical microscopy tools. A simple, yet robust, image analysis technique was developed to quantify the data obtained from SEM of the epicuticular waxes. The standardized protocols for staining the cuticle and methods developed for image analysis in this research are particularly beneficial for studying the interactions of anthropogenic substances, such as surfactants and agrochemicals, with plant surfaces. The image analysis techniques employed may also be applied to other studies on epicuticular waxes (Koch et al. 2006). Further, the study of the epicuticular waxes offers great potential for analysis of environmental pollutants (Li and Chen 2014) and may also lead to the development of novel industrial products based on inherent properties of the cuticle, such as surfaces that are self-cleaning (Barthlott and Neinhuis 1997), self-assembling (Koch et al. 2006), or display superhydrophobic properties (Samaha et al. 2012).

Acknowledgments This research was supported under Australian Research Council's Linkage Projects funding scheme (project number LP0991494). Thank you to Dr Yao Da Dong, Monash University, and Mr Chad Sayer, Nufarm Australia, for early discussions on this project.

Conflict of interest The authors declare that they have no conflict of interest.

References

Barthlott W, Neinhuis C (1997) Purity of the sacred lotus, or escape from contamination in biological surfaces. Planta 202:1–8. doi:10.1007/s004250050096

Barthlott W, Neinhuis C, Cutler D, Ditsch F, Meusel I, Theisen I, Wilhelmi H (1998) Classification and terminology of plant epicuticular waxes. Bot J Linn Soc 126:237–260. doi:10.1111/j.1095-8339.1998.tb02529.x

Beattie GA, Marcell LM (2002) Effect of alterations in cuticular wax biosynthesis on the physicochemical properties and topography of maize leaf surfaces. Plant Cell Environ 25:1–16. doi:10.1046/j.0016-8025.2001.00804.x

Broun P, Poindexter P, Osborne E, Jiang C-Z, Riechmann JL (2004) *WIN1*, a transcriptional activator of epidermal wax accumulation in *Arabidopsis*. Proc Natl Acad Sci U S A 101:4706–4711. doi:10.1073/pnas.0305574101

Buda G, Isaacson T, Matas A, Paolillo D, Rose J (2009) Three-dimensional imaging of plant cuticle architecture using confocal laser scanning microscopy. Plant J 60:378–385. doi:10.1111/j.1365-313X.2009.03960.x

Buschhaus C, Herz H, Jetter R (2007) Chemical composition of the epicuticular and intracuticular wax layers on adaxial sides of *Rosa canina* leaves. Ann Bot 100:1557–1564. doi:10.1093/aob/mcm255

Cahill D, Rookes J, Michalczyk A, McDonald K, Drake A (2002) Microtubule dynamics in compatible and incompatible interactions of soybean hypocotyl cells with *Phytophthora sojae*. Plant Pathol 51:629–640. doi:10.1046/j.0032-0862.2002.00758.x

Calbiani F, Careri M, Elviri L, Mangia A, Pistarà L, Zagnoni I (2004) Development and in-house validation of a liquid chromatography–electrospray–tandem mass spectrometry method for the simultaneous determination of Sudan I, Sudan II, Sudan III and Sudan IV in hot chilli products. J Chromatogr 1042:123–130. doi:10.1016/j.chroma.2004.05.027

Carlsson K, Mossberg K (1992) Reduction of cross-talk between fluorescent labels in scanning laser microscopy. J Mic 167:23–37. doi:10.1111/j.1365-2818.1992.tb03216.x

Chaudhury AM et al (1994) Genetic control of male fertility in *Arabidopsis thaliana*: structural analysis of premeiotic developmental mutants. Sex Plant Reprod 7:17–28. doi:10.1007/BF00241884

Chen B, Schnoor JL (2009) Role of suberin, suberan, and hemicellulose in phenanthrene sorption by root tissue fractions of switchgrass (*Panicum virgatum*) seedlings. Environ Sci Technol 43:4130–4136. doi:10.1021/es803510u

Chen B, Johnson EJ, Chefetz B, Zhu L, Xing B (2005) Sorption of polar and nonpolar aromatic organic contaminants by plant cuticular materials: role of polarity and accessibility. Environ Sci Technol 39:6138–6146. doi:10.1021/es050622q

Chen B, Li Y, Guo Y, Zhu L, Schnoor JL (2008) Role of the extractable lipids and polymeric lipids in sorption of organic contaminants onto plant cuticles. Environ Sci Technol 42:1517–1523. doi:10.1021/es7023725

Czerednik A, Busscher M, Bielen BAM, Wolters-Arts M, de Maagd RA, Angenent GC (2012) Regulation of tomato fruit pericarp development by an interplay between *CDKB* and *CDKA1* cell cycle genes. J Exp Bot 63:2605–2617. doi:10.1093/jxb/err451

Domínguez E, López-Casado G, Cuartero J, Heredia A (2008) Development of fruit cuticle in cherry tomato (*Solanum lycopersicum*). Funct Plant Biol 35:403–411. doi:10.1071/FP08018

Falk RH, Guggenheim R, Schulke G (1994) Surfactant-induced phytotoxicity. Weed Technol 8:519–525

Go YS, Kim H, Kim HJ, Suh MC (2014) *Arabidopsis* cuticular wax biosynthesis is negatively regulated by the DEWAX gene encoding an AP2/ERF-type transcription factor. The Plant Cell 26:1666–1680. doi:10.1105/tpc.114.123307

Gonthier PNG, Rettori A, Paoletti E, Gullino ML (2010) Testing *Nerium oleander* as a biomonitor for surfactant polluted marine aerosol. Int J Environ Res 4:1–10

Griffith MP, Magellan TM, Tomlinson PB (2014) Variation in leaflet structure in *Cycas* (Cycadales: cycadaceae): does anatomy follow phylogeny and geography? Int J Plant Sci 175:241–255. doi:10.1086/673884

Guzmán P, Fernández V, Khayet M, García ML, Fernández A, Gil L (2014a) Ultrastructure of plant leaf cuticles in relation to sample preparation as observed by transmission electron microscopy. Sci World J 2014:9 doi:10.1155/2014/963921

Guzmán P, Fernandez V, Graça J, Cabral V, Kayali N, Khayet M, Gil L (2014b) Chemical and structural analysis of *Eucalyptus globulus* and *E. camaldulensis* leaf cuticles: a lipidized cell wall region. Frontiers in Plant Science 5 doi:10.3389/fpls.2014.00481

Hannoufa A, McNevin J, Lemieux B (1993) Epicuticular waxes of eceriferum mutants of *Arabidopsis thaliana*. Phytochemistry 33:851–855. doi:10.1016/0031-9422(93)85289-4

Hardham A (2012) Confocal Microscopy in Plant–Pathogen Interactions. In: Bolton MD, Thomma BPHJ (eds) Plant Fungal Pathogens, vol 835. Methods in Molecular Biology. Humana Press, pp 295–309. doi:10.1007/978-1-61779-501-5_18

Herth W, Schnepf E (1980) The fluorochrome, calcofluor white, binds oriented to structural polysaccharide fibrils. Protoplasma 105:129–133. doi:10.1007/BF01279855

Jeffree CE (2007) The fine structure of the plant cuticle. In: Annual plant reviews volume 23: Biology of the plant cuticle. Blackwell Publishing Ltd, pp 11–125. doi:10.1002/9780470988718.ch2

Jenks MA, Tuttle HA, Eigenbrode SD, Feldmann KA (1995) Leaf epicuticular waxes of the *Eceriferum* mutants in *Arabidopsis*. Plant Physiol 108:369–377. doi:10.1104/pp. 108.1.369

Jenks MA, Rashotte AM, Tuttle HA, Feldmann KA (1996) Mutants in *Arabidopsis thaliana* altered in epicuticular wax and leaf morphology. Plant Physiol 110:377–385. doi:10.1104/pp. 110.2.377

Jetter R, Schaffer S (2001) Chemical composition of the *Prunus laurocerasus* leaf surface. Dynamic changes of the epicuticular wax film during leaf development. Plant Physiol 126:1725–1737. doi:10.1104/pp. 126.4.1725

Jetter R, Kunst L, Samuels AL (2007) Composition of plant cuticular waxes. In: Annual plant reviews volume 23: Biology of the plant cuticle. Blackwell Publishing Ltd, pp 145–181. doi:10.1002/9780470988718.ch4

Koch K et al (2006) Structural analysis of wheat wax (*Triticum aestivum*, c.v. 'Naturastar' L.): from the molecular level to three dimensional crystals. Planta 223:258–270. doi:10.1007/s00425-005-0081-3

Kunst L, Samuels AL (2003) Biosynthesis and secretion of plant cuticular wax. Prog Lipid Res 42:51–80. doi:10.1016/S0163-7827(02)00045-0

Lequeu J, Fauconnier M-L, Chammaï A, Bronner R, Blée E (2003) Formation of plant cuticle: evidence for the occurrence of the peroxygenase pathway. Plant J 36:155–164. doi:10.1046/j.1365-313X.2003.01865.x

Li Q, Chen B (2014) Organic pollutant clustered in the plant cuticular membranes: visualizing the distribution of phenanthrene in leaf cuticle using Two-photon confocal scanning laser microscopy. Environ Sci Technol 48:4774–4781. doi:10.1021/es404976c

Lisek J, Habdas H, Gawroński S (2002) Relationship between selected morphological, anatomical and cytological characteristics of leaves and the level of tolerance to herbicides in strawberry cultivars. Acta Physiol Plant 24:371–378. doi:10.1007/s11738-002-0032-6

Ménard R, Verdier G, Ors M, Erhardt M, Beisson F, Shen W-H (2014) Histone H2B monoubiquitination is involved in the regulation of cutin and wax composition in *Arabidopsis thaliana*. Plant Cell Physiol 55:455–466. doi:10.1093/pcp/pct182

Millar AA, Clemens S, Zachgo S, Giblin EM, Taylor DC, Kunst L (1999) *CUT1*, an arabidopsis gene required for cuticular wax biosynthesis and pollen fertility, encodes a very-long-chain fatty acid condensing enzyme. Plant Cell 11:825–838. doi:10.1105/tpc.11.5.825

Nadiminti PP, Dong YD, Sayer C, Hay P, Rookes JE, Boyd BJ, Cahill DM (2013) Nanostructured liquid crystalline particles as an alternative delivery vehicle for plant agrochemicals. ACS Appl Mater & Interfaces 5:1818–1826. doi:10.1021/am303208t

Pathan AK, Bond J, Gaskin RE (2008) Sample preparation for scanning electron microscopy of plant surfaces—Horses for courses. Micron 39:1049–1061. doi:10.1016/j.micron.2008.05.006

Peirson B, Owen H, Feldmann K, Makaroff C (1996) Characterization of three male-sterile mutants of *Arabidopsis thaliana* exhibiting alterations in meiosis. Sex Plant Reprod 9:1–16. doi:10.1007/BF00230361

Poulios I, Avranas A, Rekliti E, Zouboulis A (2000) Photocatalytic oxidation of Auramine O in the presence of semiconducting oxides. J Chem Technol Biotechnol 75:205–212. doi:10.1002/(SICI)1097-4660(200003)75:3<205::AID-JCTB201>3.0.CO;2-L

Rascio A, Rascio N, Rinaldi M, Valentini M (2014) Functional, histological and biomechanical characterization of wheat water-mutant leaves Physiol Plant:n/a-n/a doi:10.1111/ppl.12280

Rashotte AM, Jenks MA, Thanh DN, Feldmann KA (1997) Epicuticular wax variation in ecotypes of *Arabidopsis thaliana*. Phytochemistry 45:251–255. doi:10.1016/S0031-9422(96)00792-3

Riederer M (2007) Introduction: Biology of the Plant Cuticle. In: Annual plant reviews volume 23: Biology of the plant cuticle. Blackwell Publishing Ltd, pp 1–10. doi:10.1002/9780470988718.ch1

Ruberti C et al. (2014) Mitochondria Change Dynamics and Morphology during Grapevine Leaf Senescence PLoS One 9:e102012 doi:10.1371/journal.pone.0102012

Samaha MA, Tafreshi HV, Gad-el-Hak M (2012) Superhydrophobic surfaces: from the lotus leaf to the submarine. Comptes Rendus Mécanique 340:18–34. doi:10.1016/j.crme.2011.11.002

Schneider CA, Rasband WS, Eliceiri KW (2012) NIH image to ImageJ: 25 years of image analysis. Nat Methods 9:671–675. doi:10.1038/nmeth.2089

Serrano M, Coluccia F, Torres M, L'Haridon F, Metraux J (2014) The cuticle and plant defense to pathogens front. Plant Sci 5:274. doi:10.3389/fpls.2014.00274

Tamura H, Knoche M, Bukovac MJ (2001) Evidence for surfactant solubilization of plant epicuticular wax. J Agric Food Chem 49:1809–1816. doi:10.1021/jf000608r

Wilson SM, Bacic A (2012) Preparation of plant cells for transmission electron microscopy to optimize immunogold labeling of carbohydrate and protein epitopes. Nat Protoc 7:1716–1727. doi:10.1038/nprot.2012.096

Xue Y, Xiao S, Kim J, Lung S-C, Chen L, Tanner JA, Suh, MC, Chye, M-L (2014) *Arabidopsis* membrane-associated acyl-CoA-binding protein ACBP1 is involved in stem cuticle formation. J Exp Bot doi:10.1093/jxb/eru304

Yeats TH, Rose JKC (2013) The formation and function of plant cuticles. Plant Physiol 163:5–20. doi:10.1104/pp. 113.222737

Yeats TH, Martin LBB, Viart HMF, Isaacson T, He Y, Zhao L, Matas AJ, Buda GJ, Domozych DS, Clausen MH, Rose JKC (2012) The identification of cutin synthase: formation of the plant polyester cutin Nat Chem Biol 8:609–611 doi:http://www.nature.com/nchembio/journal/v8/n7/abs/nchembio.960.html#supplementary-information

Zhou X, Jenks M, Liu J, Liu A, Zhang X, Xiang J, Zou J, Peng Y, Chen X (2014) Overexpression of transcription factor OsWR2 regulates wax and cutin biosynthesis in rice and enhances its tolerance to water deficit. Plant Mol Biol Rep 32:719–731. doi:10.1007/s1-013-0687-8